IEEE Open Journal of
Antennas and Propagation

Received 12 January 2021; revised 8 February 2021; accepted 10 February 2021. Date of publication 24 February 2021; date of current version 9 March 2021.

Digital Object Identifier 10.1109/OJAP.2021.3061961

A Novel Dual-Polarized Wideband and Miniaturized Low Profile Magneto-Electric Dipole Antenna Array for mmWave 5G Applications

YIN CHEN CHANG, CHING CHENG HSU, M. IDREES MAGRAY (Graduate Student Member, IEEE), HSU YUNG CHANG, AND JENN-HWAN TARNG (Senior Member, IEEE)

Institute of Communication Engineering, College of Electrical and Computer Engineering, National Chiao Tung University, Hsinchu City 300, Taiwan

CORRESPONDING AUTHOR: M. I. MAGRAY (e-mail: idreesmagrey@gmail.com)

This work was supported in part by the "Center for mmWave Smart Radar Systems and Technologies" through the Featured Areas Research Center Program within the framework of the Higher Education Sprout Project by the Ministry of Education (MOE), Taiwan, and in part by MOST, Taiwan, under Grant MOST 109-2634-F-009-030.

ABSTRACT A Ka-band dual-polarized low profile magneto-electric (ME) dipole antenna with wide operational bandwidth is proposed in this paper. A thin substrate with two-stage meandered vias is utilized for realization of the proposed antenna. The meandered vias aid in compensation of phase difference caused due to utilization of thin substrate. The thickness of proposed antenna is reduced from 0.25 λ_g to 0.11 λ_g by using these two-stage meandered vias. The low profile antenna topology results in bandwidth reduction which is neutralized by introducing asymmetric slots in the ground plane. Shorting pins are inserted for elimination of higher order TM_{21} mode of Ka-band that results in a uniform broadside radiation pattern due to excitation of fundamental TM_{10} mode. The proposed antenna covers whole Ka-band with operating frequencies from 26 – 42 GHz. A 1 × 4 antenna array is also designed and fabricated with a reasonable gain of 12.06 dBi and stable radiation patterns. Simulated and measurement results are presented with detailed justification.

INDEX TERMS Low profile, wideband, dual-polarization, magneto-electric (ME) dipole antenna, mmWave 5G.

I. INTRODUCTION

THE EMERGENCE of fifth generation (5G) cellular networks has led widespread attention to millimeter-wave (mmWave) broadband antennas due to demand for high data rates. The mmWave 5G broadband antennas should cover the candidate frequency bands for 5G communication which include 28 and 38 GHz bands of Ka-band [1]. Besides wider operating bandwidth, dual-polarization is another feature of antennas which improves channel capacity and minimizes multipath fading [2].

Various techniques have been investigated for antennas to possess dual-polarization with wider impedance bandwidth like in [3]–[5], but the antennas bear large thickness which could be inappropriate for mobile terminals since the form factor for future millimeter devices is needed to be small. A metasurface based ultra-wideband antenna with fractional bandwidth of more than 60% has been explored in [6], but the antenna suffers from low gain which limits its applicability for mmWave 5G applications. For wideband performance with stable radiation patterns, magneto-electric (ME) dipole antenna [7] has attracted a lot of attention due to its suitability for mmWave 5G applications. However, the ME-dipole antenna suffers from large thickness for its realization, which is quarter wavelength (0.25 λ_0) between the radiating patches and ground plane. Various methods have been proposed for obtaining low profile ME-dipole antennas like folded metal wall based magnetic dipole [8], electric dipole with etched U-shaped slot [9] and magnetic dipole formed by obtuse triangular shaped metal [10]. Although the overall thickness of ME-dipole antenna has been reduced but these methods tend to sacrifice the operating bandwidth of antenna. A folded shorted patch based ME-dipole antenna has also been proposed in [11], however the antenna wouldn't be suitable for dual-polarization due to its asymmetric nature. Also, the level of miniaturization in antenna's thickness isn't that

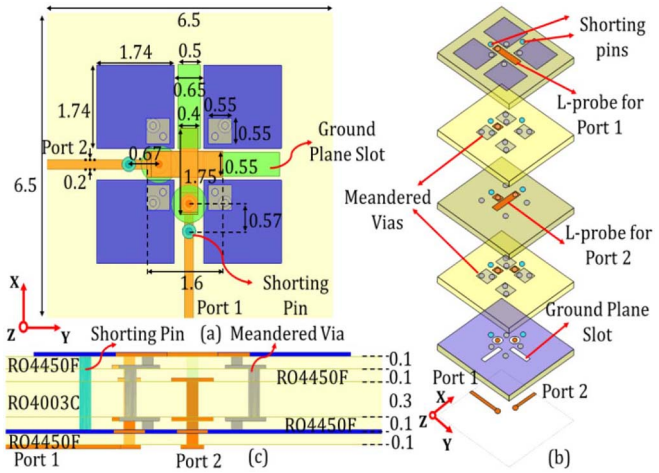

FIGURE 1. Schematics of the proposed dual-polarized ME-dipole antenna (a) top view, (b) perspective view and (c) side view (All dimensions are in mm).

much significant. Furthermore, a wideband dual-polarized ME-dipole antenna array for Ka-band wireless applications has been investigated in [12]. Even though the fractional bandwidth of antenna is more than 40% and height of antenna is only 0.12 λ_0, but the cost of antenna is relatively high since the low temperature co-fired ceramic (LTCC) material has been used for its implementation rather than printed circuit board (PCB). Also, the high dielectric constant, $\varepsilon_r = 5.9$ of LTCC helps in the reduction of overall height of antenna. Designing a PCB based low profile wideband ME-dipole antenna is still a challenge and therefore a multilayered PCB based novel miniaturized compact wideband ME-dipole antenna is proposed. The proposed antenna utilizes height of only 0.06 λ_0 at 26 GHz with fractional bandwidth of more than 45%. The two-stage meandered vias are utilized for miniaturization. Ground slots and shorting pins are introduced for compensation of bandwidth reduction and low gain at high frequencies respectively. Section II describes the design and characterization of single element dual-polarized ME-dipole antenna, followed by design of one-dimensional ME-dipole antenna array in Section III.

II. LOW PROFILE AND WIDEBAND DUAL-POLARIZED ME-DIPOLE ANTENNA DESIGN

The geometry of the proposed antenna is illustrated in Fig. 1 with detailed configuration parameters. The proposed antenna is realized by using Rogers RO4003C and RO4450F multi-layered structure with relative permittivity (ε_r) of 3.38 $\pm$ 0.05 and 3.52 $\pm$ 0.05 respectively. The overall topology of ME-dipole antenna consumes height of only 0.7 mm, which equals to 0.06 λ_0 at 26 GHz. Six metallic layers are utilized in the design process in which four square patches are etched at the top layer which work as a pair of electric dipoles. Two-stage meandered vias are introduced for realization of magnetic dipole with meandering performed at second and fourth stage of metallic layers. A shorting

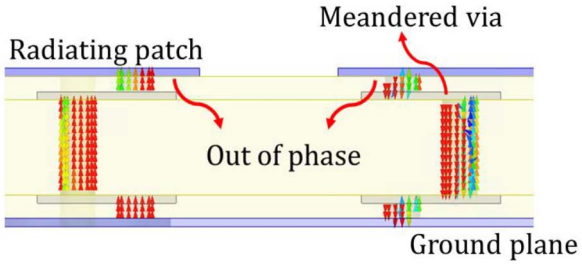

FIGURE 2. Current distribution in meandered vias.

pin is also incorporated between top and ground/fifth layer for attaining broadside stable radiation patterns with optimal gain at higher frequencies. Furthermore, two asymmetric ground slots are also added for obtaining wider impedance bandwidth. The proposed antenna is fed by two orthogonal L-shaped probes placed at different heights for exciting the radiation patches with different polarizations thereby achieving dual-polarization. The probes are connected with 50 Ω microstrip transmission lines placed at the bottom layer of multilayered structure.

Conventionally, the ME-dipole antenna has two resonant modes in which electric dipole resonates at lower operating frequencies and magnetic dipole at higher frequencies [13]. The resonances of both electric and magnetic dipoles are mainly governed by the length of radiating patches and height of the shorted patch radiator, respectively. The magnetic dipole therefore decides the height of ME-dipole antennas which is a quarter wavelength (0.25 λ_0) between the radiating patches and ground plane. Reducing the thickness of ME-dipole antenna will decrease phase difference between radiating apertures that will result in the resonance of magnetic dipole at higher frequencies that are out of the targeting bands. Thus, for compensation of phase difference between radiating apertures, the two-stage meandered vias are introduced as depicted in Fig. 2. The meandered vias extend current path thereby maintaining required 180° phase difference between two planar radiating patches. The overall thickness of ME-dipole antenna is reduced from 0.25 λ_g to 0.11 λ_g, which accounts for 56% to obtain the low profile antenna topology. Since the two-stage meandered vias are symmetrical, dual-polarization is easily achieved.

The decrease in overall thickness of ME-dipole antenna and the implementation of meandered vias will result in impedance mismatch of electric dipole. The impedance mismatch will therefore result in bandwidth reduction of ME-dipole antenna. This mainly occurs by increase in induced current of the electric dipole on ground plane, and its current path that becomes smaller than path followed by meandered vias thereby causing a frequency shift of electric dipole from 28 GHz to higher frequency 32 GHz as illustrated in Fig. 3 (a). This phenomenon can be noticed from Fig. 3 (b), (c) and (d), which shows the current distribution of ground plane with comparatively thick and thin substrate heights respectively. From Fig. 3 (b), the current

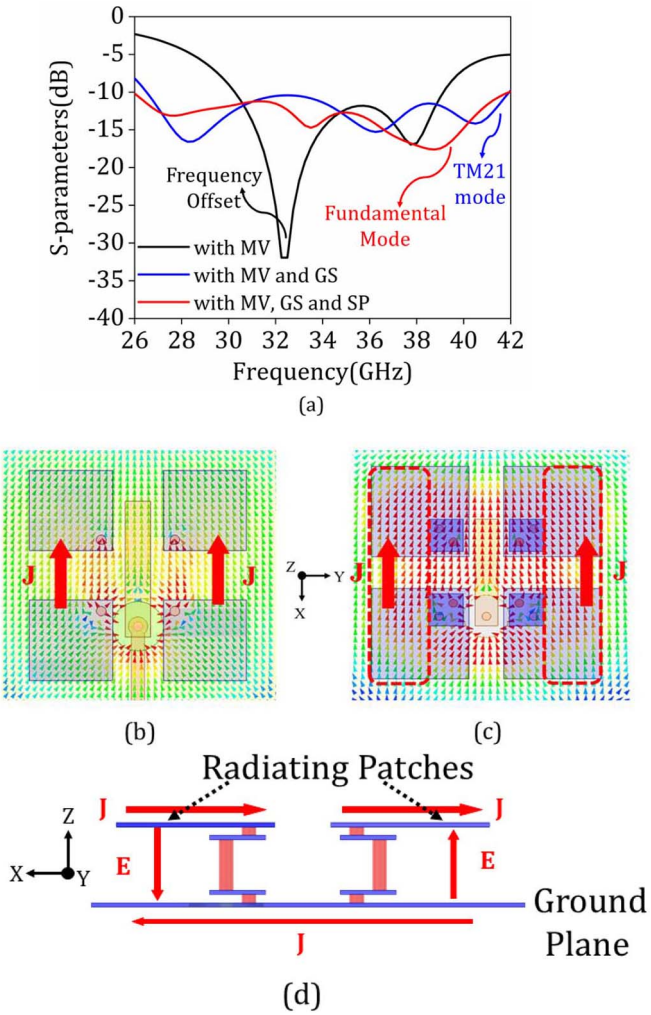

FIGURE 3. (a) S-parameters with successive modification in proposed antenna topology (MV = Meandered vias, GS = ground slots and SP = shorting pins), (b) Current distribution of the ground plane at 32 GHz with substrate height, h = 1.3 mm, (c) Current distribution at 32 GHz with substrate height, h = 0.6 mm and (d) Realization of current path.

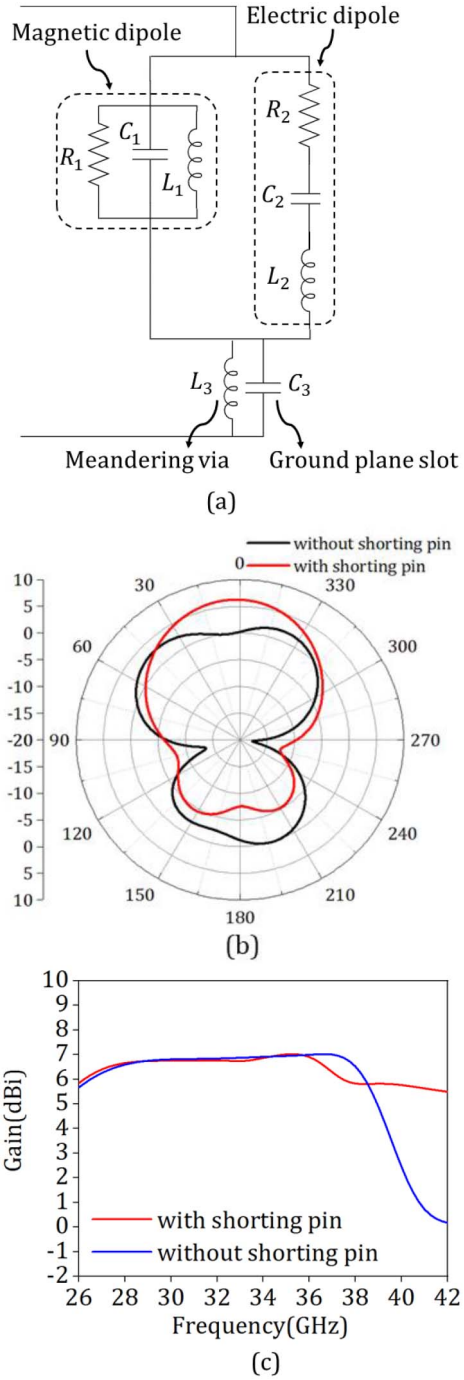

FIGURE 4. (a) Equivalent circuit, (b) radiation patterns at 41 GHz and (c) simulated gain of proposed antenna.

path is mainly concentrated from via to via that signifies minimal coupling from radiating patches to ground plane. On the other hand, strong coupling can be observed between radiating patches and ground plane in Fig. 3 (c), which generates additional shorter current path than meandered vias. Moreover, Fig. 3 (d) depicts the side-view of proposed ME-dipole antenna in which a proper current path is generated due to induced coupling from radiating patches and ground plane. Therefore, this shorter current path results in frequency shift of electric dipole from 28 GHz to 32 GHz.

The equivalent circuit of the proposed ME-dipole antenna is depicted in Fig. 4(a). The magnetic dipole can be represented by a parallel resonant circuit and electric dipole can be portrayed by a series resonant circuit. Meandered vias that connect the radiating patches and ground plane can be represented by an inductance and ground plane slot by a parallel capacitance. The meandered vias excite higher order TM_{21} mode that causes non-boresight radiation at higher frequencies. In order to increase the path for induced current on the ground plane, a rectangular shaped slot is etched on the ground plane that nullifies effect of additional current hence shifting the lower operating frequency to 28 GHz as depicted in Fig. 3(a). The ground slots are added asymmetrically opposite to L-shaped probe feeds of the dual-polarized ME-dipole antenna for preventing any disturbance in mode excitation between L-shaped probe and the ground plane. The impedance matching of magnetic dipole is not affected

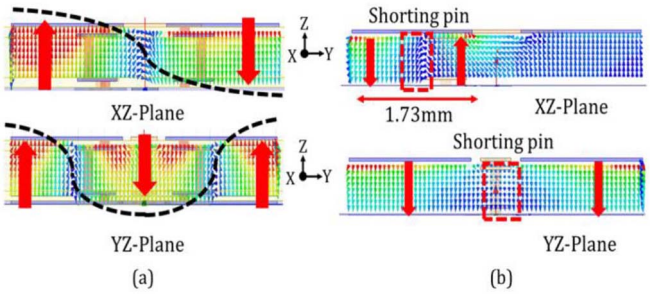

FIGURE 5. Electric field distribution (a) without shorting pin and (b) with shorting pin.

as the current path for magnetic dipole remains unaltered in the presence of the slots. In addition to lower frequency resonance, the ground slots provide parallel capacitance that resonates the ME-dipole at higher order TM_{21} mode as well thereby covering higher frequencies. However, radiation patterns are bi-lobed at higher frequencies which produces radiation null at boresight direction thereby resulting in low gain as presented in Fig. 4 (b) and (c) respectively. The radiation null at the boresight direction is due to current reversal on the four radiating patches.

For obtaining stable radiation patterns with optimal gain at higher frequencies, shorting pins are introduced. The proposed ME-dipole antenna utilizes minimum number of shorting pins for elimination of TM_{21} mode and accordingly produces fundamental TM_{10} mode. Compared with TM_{21} mode which produces bi-lobed radiation pattern, the fundamental mode generates the main radiation beam along the boresight direction with high front-to-back ratio. Each polarization needs a separate shorting pin at a proper position where electric field strength is high for eliminating TM_{21} mode effectively. Therefore, shorting pins are added near the L-probes for coupling maximum electric field to the nearby pair of radiating patches. The shorting pin unifies electrical field distribution and changes TM_{21} mode electric field distribution as shown in Fig. 5 (a) to a uniform electric field distribution as illustrated in Fig. 5 (b).

Shorting pins are not connected with radiating patches for avoiding any sort of impedance mismatch. The coupled electric field induces currents on radiating patches which excites the fundamental TM_{10} mode similar to rectangular patch antenna. The current distribution is mainly concentrated on a pair of radiating patches lying closer to shorting pin as shown in Fig. 6 (c). The excitation of fundamental mode at higher frequencies enhances the gain of antenna by around 5 dB and stabilizes the radiation patterns to boresight direction as depicted in Fig. 4 (c). Also, the impedance bandwidth is enhanced by covering 26 GHz frequency band which accounts for 5% increase in bandwidth therefore covering the whole Ka-band as illustrated in Fig. 3 (a). Shorting pin implementation does not increase the antenna area or thickness which is very advantageous for array design. Fig. 6 illustrates the operation of proposed ME-dipole antenna on excitation

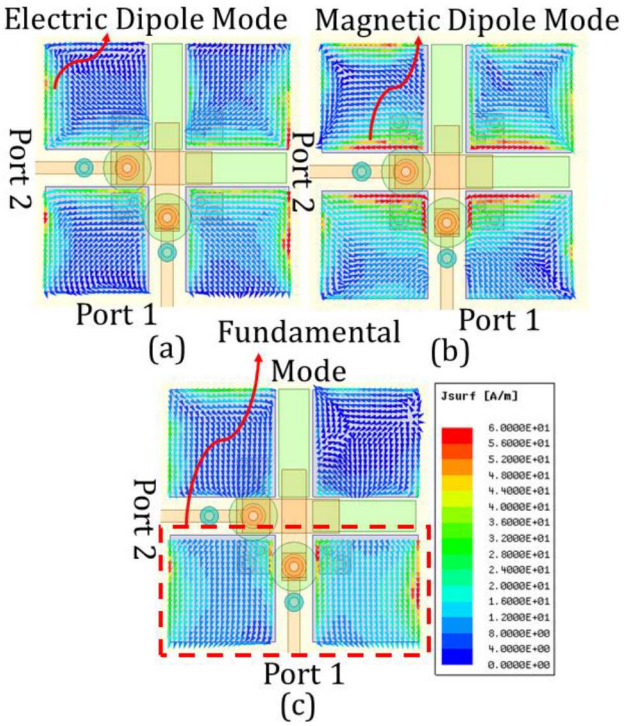

FIGURE 6. Current distribution of the proposed ME-dipole antenna when Port 1 is excited at (a) 28 GHz, (b) 38 GHz and (c) 41 GHz.

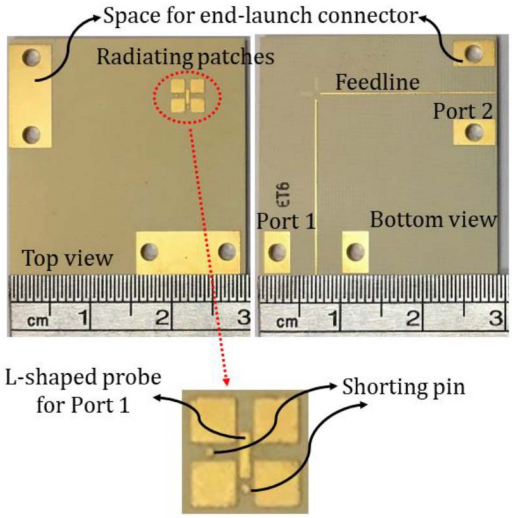

FIGURE 7. Photographs of the fabricated dual-polarized ME-dipole antenna.

of three different modes: electric dipole, magnetic dipole and fundamental mode.

All full-wave antenna simulations were performed using high-frequency structural simulator (HFSS). The proposed dual-polarized ME-dipole antenna is fabricated and photographs are shown in Fig. 7. Area of the substrate and length of feedline are extended for accommodating 2.92 mm end-launch connector used for antenna performance measurements. The extended area will prevent any beam tilt in

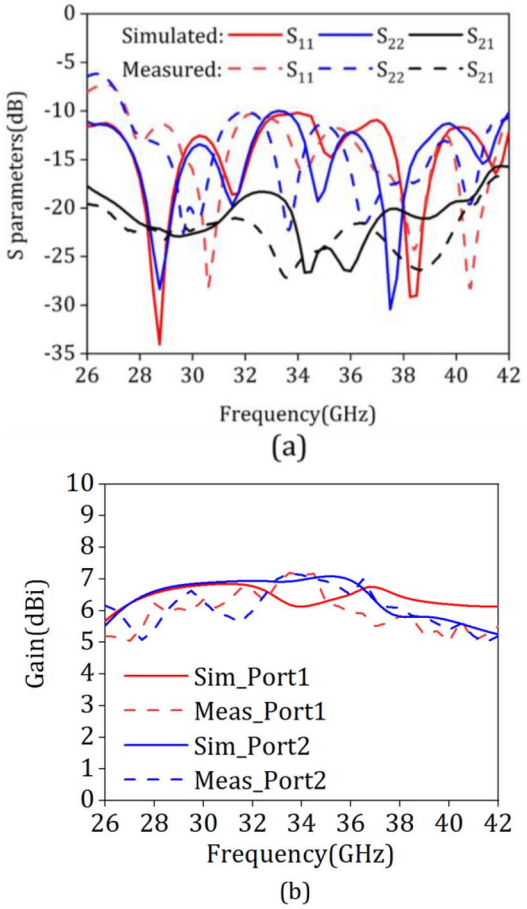

FIGURE 8. Simulated and measured (a) S-parameters and (b) broadside gain of proposed dual-polarized ME-dipole antenna.

broadside direction due to reflection from a bulky end-launch connector.

The simulated and measured S-parameters of proposed dual-polarized ME-dipole antenna are depicted in Fig. 8 (a). Both the antenna ports cover whole Ka-band with operating frequencies ranging from 26 – 42 GHz with fractional bandwidth of 47.1%. The proposed antenna operates at three modes: electric dipole mode at lower operational frequencies, magnetic dipole mode at mid-operational frequencies and a fundamental mode at higher frequencies. It can be noticed that there is a frequency shift in measured S-parameters compared with simulated ones, which is mainly due to significant difference of dielectric constants between fabricated multilayered structure and simulated substrate topology. The mutual coupling between two orthogonal ports is less than 17 dB in the entire operating band. The isolation can be enhanced by increasing the vertical distance between L-shaped probes but that will reduce the operational bandwidth of Port 2. Therefore, there is a tradeoff between isolation and impedance bandwidth.

Fig. 8(b) presents simulated and measured broadside gain of the proposed dual-polarized ME-dipole antenna. Peak gain of around 7 dBi is obtained for both the orthogonal ports. It

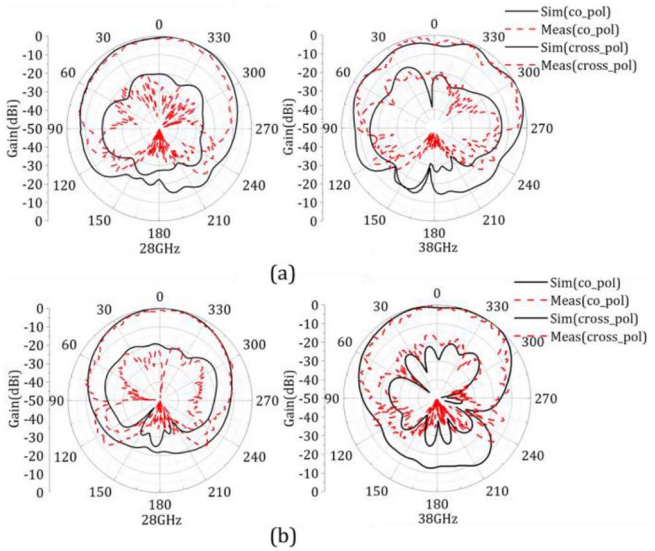

FIGURE 9. Simulated and measured radiation patterns of the proposed antenna in (a) E-plane (XZ-plane) and (b) H-plane (YZ-plane).

is noticed that there is a slight gain drop at higher frequencies that is due to decrease in effective radiating aperture since the proposed antenna operates at fundamental TM_{10} mode. This mode only excites a pair of radiating patches on the top plane, therefore leading to slight gain drop at higher frequencies.

The simulated and measured co-pol and cross-pol radiation patterns of the proposed antenna in both the principal planes when Port 1 is excited are presented in Fig. 9. Since the antenna is symmetrical, therefore radiation patterns of Port 2 are almost identical to those of Port 1. Also, the benefit of using dual-polarization in ME-dipole antenna is that radiation patterns are almost similar for both the antenna ports [12], [14]. The radiation patterns are stable in nature with similar E-plane and H-plane radiation patterns. Half power beamwidth (HPBW) of proposed antenna is around 60 degrees and front-to-back ratio (FBR) is more than 14 dB. Cross-polarization of less than −18 dB is obtained over the entire operating frequency band indicating a strongly linearly polarized antenna. Discrepancies between simulated and measured data could be attributed to alignment errors between transmitting antenna-under-test (AUT) and receiving high gain horn antenna.

Cross-polarization is slightly high and one of the possible reasons could be attributed to unwanted radiations caused by exposed L-shaped probes in the both polarizations, whose radiation level increases with frequency. Moreover, excitation of higher-order modes in the proposed dual-polarized ME-dipole antenna would also degrade the polarization purity. Some approaches do exist for reducing the cross-polarization in the proposed antenna, but there are some trade-offs. For example, utilization of differential feeding network will suppress higher-order modes thereby enhancing polarization purity [15]. However, realization of the differential feeding will require two feedlines

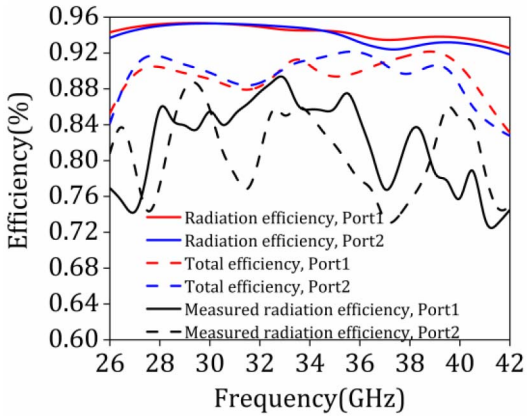

FIGURE 10. Radiation and total efficiency of the proposed single element ME-dipole antenna.

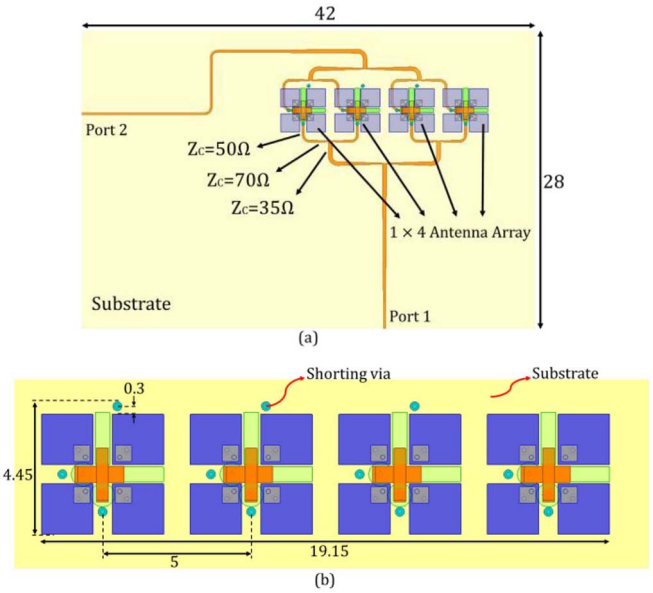

FIGURE 11. Schematics of the proposed dual-polarized ME-dipole antenna array (a) top view and (b) magnified view of antenna elements (All dimensions are in mm).

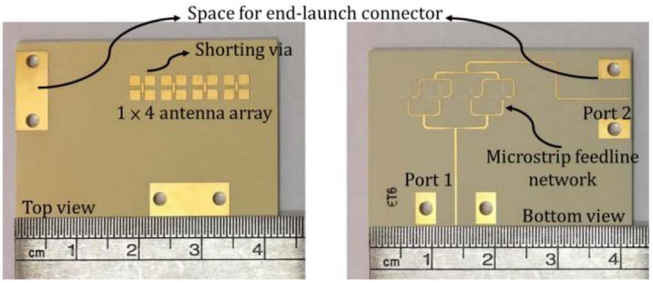

FIGURE 12. Photographs of the proposed fabricated antenna array.

having same signal amplitude and phase difference of 180° with respect to each other. The implementation of differential feeding in the proposed antenna will result in additional feeding network thereby increasing the overall size of antenna. Another method is to decrease the overall thickness of proposed antenna, which will suppress transverse currents of the higher-order modes. However, the decrease in antenna thickness will result in reduction of overall operating bandwidth of proposed antenna. In general, it is common to have cross-polarization value of around −16 dB in dual-polarized and wideband ME-dipole antennas like in [12], [16]. Furthermore, simulated and measured radiation efficiency and total efficiency of more than 91% and 83% respectively is obtained across the entire operational frequency band for both the orthogonal ports respectively as depicted in Fig. 10. Radiation efficiency is calculated by, $\eta_{rad} = \frac{P_{radiated}}{P_{input}}$ and total efficiency is evaluated by, $\eta_{total} = \eta_{rad} \times (1 - S_{11}{}^2)$. In addition to losses contributed within the antenna topology, total efficiency takes into account losses at the input terminals in comparison with radiation efficiency thereby causing a comparatively larger drop in values of total efficiency.

III. LOW PROFILE AND WIDEBAND DUAL-POLARIZED ANTENNA ARRAY

A 1 × 4 linear antenna array composed by the proposed dual-polarized ME-dipole antennas discussed in Section II is designed for Ka-band operation, which include 28 and 38 GHz mmWave 5G frequencies. Schematics of the proposed antenna array topology is illustrated in Fig. 11. The spacing between antenna elements is 5 mm which corresponds to 0.55 λ_0 at center frequency. A via is incorporated in-between the rectangular patches for avoiding parasitic coupling that will lead to impedance mismatch and hence reduces operational bandwidth.

Fig. 12 shows photographs of fabricated dual-polarized ME-dipole antenna array. The feeding network is composed of truncated microstrip lines optimized for wider impedance bandwidth. A physical offset is introduced in feedline of Port 2 that is primarily done for reduction of physical size of antenna array, otherwise size of multilayered structure would have been increased for accommodating bulky 2.92 mm end-launch connector.

The simulated and measured S-parameters of proposed antenna array are depicted in Fig. 13 (a) which are in good agreement with each other. The proposed antenna array operates on whole Ka-band for both the orthogonal ports with simulated and measured impedance bandwidth ranging from 26 – 42 GHz. The measured isolation between orthogonal ports is more than 18 dB across the entire operational frequency band. Fig. 13 (b) depicts the simulated and measured gain of proposed antenna array. Comparatively, a slight gain drop can be noticed which can be attributed to usage of shorting vias between antenna elements. Shorting vias will reduce the coupling between various antenna elements and henceforth increase the isolation, however coupling to vias will degrade the overall gain performance of antenna array. The peak gain is 12.06 dBi and 11 dBi for Port 1 and Port 2 respectively. Gain variation of around 3 dB is

TABLE 1. Comparison of the proposed dual-polarized antenna array with other recently reported antenna arrays.

REF	TOA	No. of elements	OF (GHz)	Thickness of Antenna (λ_0)	OM	Cost	FB	PG(dBi)	3-dB GBW	Dual-pol
[4]	Yagi-Uda	4	36	0.23	1	Low	23.7%	11	23.7%	88%
[9]	ME-Dipole	16	32	0.13	3	Low	19.1%	20	19.1%	NA
[12]	ME-Dipole	16	28, 38	0.095	2	High	45%	16	39.4%	84%
[14]	ME-Dipole	1	3.55, 4.05	0.11	3	Low	27.6%	8.2	27.6%	93%
[17]	ME-Dipole	40	60	0.17	3	Low	30.7%	25.1	25.1%	80%
[18]	SIW horn	4	28	0.1	2	Low	7.1%	8.14	7.1%	NA
[19]	ME-Dipole	4	45	0.18	2	Low	36.6%	12.2	23.96%	85%
[20]	Folded Slot	4	38	0.11	1	High	18.6%	7.7	NA	NA
PW	ME-Dipole	4	28, 38	0.06	3	Low	47.1%	12.06	40%	95%

*TOA = Type of Antenna, OF = Operating Frequency, OM = Operating Mode(s), FB = Fractional Bandwidth, PG = Peak Gain, GBW = Gain Bandwidth, NA = Not Available and PW = Proposed Work

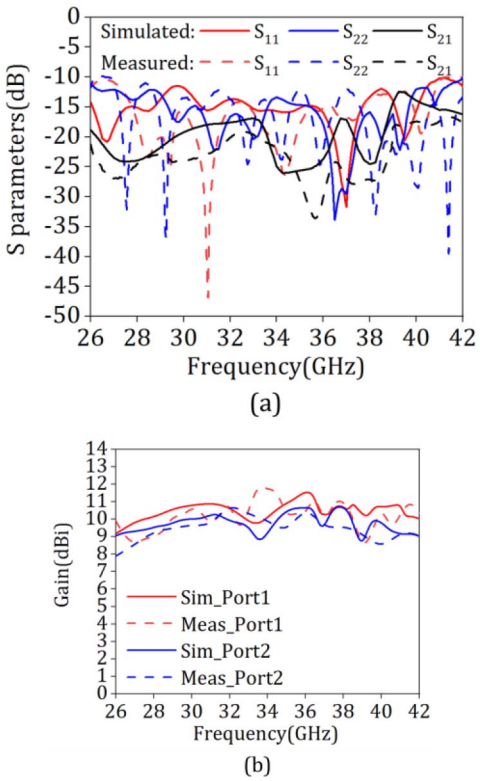

FIGURE 13. (a) S-parameters and (b) gain of the proposed antenna array.

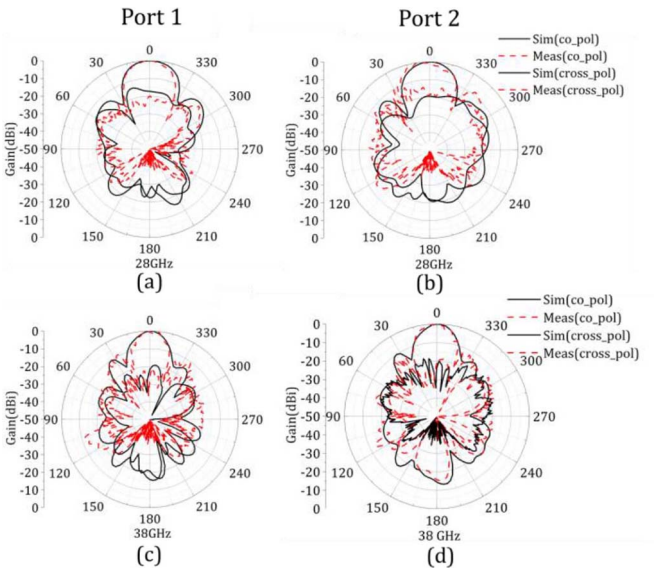

FIGURE 14. Simulated and measured radiation patterns of the proposed antenna array in E-plane (XZ-plane) for Port 1 ("a" and "c") and H-plane (YZ-plane) for Port 2 ("b" and "d").

obtained for both the orthogonal ports over the entire operating wideband indicating high pattern integrity. Furthermore, fluctuating gain performance of the presented ME-dipole antenna array could be attributed to coupling between various antenna elements.

The simulated and measured radiation patterns of the proposed antenna array are depicted in Fig. 14. Stable unidirectional broadside radiation patterns are achieved in both the principal planes with front-to-back ratio of more than 18 dB. Cross-polarization is less than −16 dB, a 2-dB increase compared with the single element case. It is because of the longer feeding network with specific bends and discontinuities that cause unwanted radiations. Simulated and measured radiation efficiency and total efficiency of more than 82% and 73% is attained for both the polarizations of proposed antenna array respectively as presented in Fig. 15. Radiation efficiency of Port 1 of proposed antenna array is slightly higher in the lower frequencies than single element dual-polarized ME-dipole antenna which is due to comparatively low value of input reflection co-efficient of antenna array at these frequencies. In addition to this, a relative difference of around 0.04% in radiation efficiencies of antenna array over a whole frequency range can be noticed between Port 1 and Port 2. This could be attributed to the additional loss caused by increase in length of feedline of Port 2.

Table 1 illustrates the performance characteristics of proposed linear dual-polarized ME-dipole antenna array compared with the other antenna arrays. It is evident that proposed dual-polarized antenna array attains

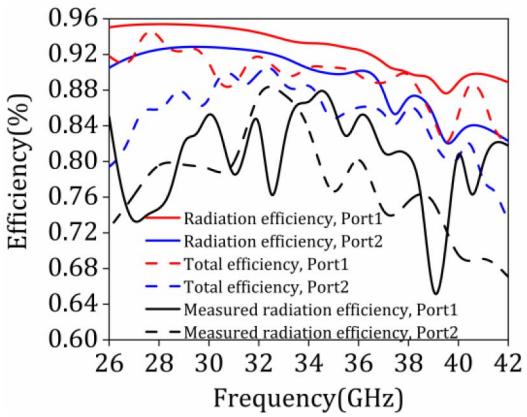

FIGURE 15. Radiation and total efficiency of the proposed antenna array.

wide impedance bandwidth with comparatively very low profile.

IV. CONCLUSION

This paper presents a wideband and low-profile dual-polarized ME-dipole antenna array operating for whole Ka-band. The meandered vias are introduced to achieve low-profile topology of 0.11 λ_g. The ground plane slots and shorting pins are properly realized for wide impedance bandwidth of 47.1 % and stable radiation patterns in boresight direction, respectively. A 1 $\times$ 4 ME-dipole antenna array with wide impedance bandwidth and high isolation is also investigated. The proposed dual-polarized ME-dipole antenna array that overcomes the challenges of low thickness and wide impedance bandwidth would be an attractive candidate for millimeter-wave 5G applications.

REFERENCES

[1] C.-X. Wang *et al.*, "Cellular architecture and key technologies for 5G wireless communication networks," *IEEE Commun. Mag.*, vol. 52, no. 2, pp. 122–130, Feb. 2014.
[2] K.-L. Wong, *Compact and Broadband Microstrip Antennas*. Hoboken, NJ, USA: Wiley, 2002.
[3] H. Li, Y. Li, L. Chang, W. Sun, X. Qin, and H. Wang, "Wideband dual-polarized endfire antenna array with overlapped apertures and small clearance for 5G millimeter wave applications," *IEEE Trans. Antennas Propag.*, vol. 69, no. 2, pp. 815–824, Feb. 2021.
[4] Y.-W. Hsu, T.-C. Huang, H.-S. Lin, and Y.-C. Lin, "Dual-polarized Quasi Yagi–Uda antennas with endfire radiation for millimeter-wave MIMO terminals," *IEEE Trans. Antennas Propag.*, vol. 65, no. 12, pp. 6282–6289, Dec. 2017.
[5] B. Feng, X. He, J.-C. Cheng, and C.-Y.-D. Sim, "Dual-wideband dual-polarized metasurface antenna array for the 5G millimeter wave communications based on characteristic mode theory," *IEEE Access*, vol. 8, pp. 21589–21601, 2020.
[6] C.-C. Hsu, N.-C. Liu, S.-J. Wu, and J.-H. Tarng, "An ultra-wideband millimeter wave aperture-coupled patch antenna using a comb-shaped metasurface," in *Proc. IEEE Asia-Pac. Microw. Conf. (APMC)*, Singapore, 2019,pp. 658–660.
[7] K. M. Luk and H. Wong, "A new wideband unidirectional antenna element," *Int. J. Microw. Opt. Technol.*, vol. 1, no. 1, pp. 35–44, Jun. 2006.
[8] W. Wang, M. Tang, Z. Shao, and Y. Zhang, "A low-profile magneto-electric dipole antenna with parasitic patches for millimeter-wave antenna-in-package applications," in *Proc. Photon. Electromagn. Res. Symp. Fall (PIERS-Fall)*, Xiamen, China, 2019, pp. 3016–3019.
[9] G. Yang, J. Zhang, and Z. Zhou, "Low-profile broadband aperture coupled magneto-electric dipole array antenna for millimetre-wave applications," *Electron. Lett.*, vol. 56, no. 6, pp. 271–273, 2020.
[10] C. Ding and K.-M. Luk, "Low-profile magneto-electric dipole antenna," *IEEE Antennas Wireless Propag. Lett.*, vol. 15, pp. 1642–1644, 2016.
[11] L. Ge and K. M. Luk, "A simple low-profile magneto-electric dipole antenna element," in *Proc. IEEE Int. Wireless Symp.*, 2013, pp. 1–3.
[12] Y. Li, C. Wang, and Y. X. Guo, "A Ka-band wideband dual-polarized magnetoelectric dipole antenna array on LTCC," *IEEE Trans. Antennas Propag.*, vol. 68, no. 6, pp. 4985–4990, Jun. 2020.
[13] M. Li and K.-M. Luk, "Wideband magnetoelectric dipole antennas with dual polarization and circular polarization," *IEEE Antennas Propag. Mag.*, vol. 57, no. 1, pp. 110–119, Feb. 2015.
[14] S. J. Yang, Y. M. Pan, Y. Zhang, Y. Gao, and X. Y. Zhang, "Low-profile dual-polarized filtering magneto-electric dipole antenna for 5G applications," *IEEE Trans. Antennas Propag.*, vol. 67, no. 10, pp. 6235–6243, Oct. 2019.
[15] B. Feng, T. Luo, T. Zhou, and C.-Y.-D. Sim, "A dual-polarized antenna with low cross polarization, high gain, and isolation for the fifth-generation array/multiple-input multiple-output communications," *Int. J. RF Microw. Comput. Aided Eng.*, vol. 31, no. 2, 2021, Art. no. e22278.
[16] Y. Li and K.-M. Luk, "60-GHz dual-polarized two-dimensional switch-beam wideband antenna array of aperture-coupled magneto-electric dipoles," *IEEE Trans. Antennas Propag.*, vol. 64, no. 2, pp. 554–563, Feb. 2016.
[17] G.-H. Sun and H. Wong, "A planar millimeter-wave antenna array with a pillbox-distributed network," *IEEE Trans. Antennas Propag.*, vol. 68, no. 5, pp. 3664–3672, May 2020.
[18] J. Zhang, K. Zhao, L. Wang, S. Zhang, and G. F. Pedersen, "Dual-polarized phased array with end-fire radiation for 5G handset applications," *IEEE Trans. Antennas Propag.*, vol. 68, no. 4, pp. 3277–3282, Apr. 2020.
[19] Z.-C. Hao and B.-W. Li, "Developing wideband planar millimeter-wave array antenna using compact magneto-electric dipoles," *IEEE Antennas Wireless Propag. Lett.*, vol. 16, pp. 2102–2105, 2017.
[20] J. Park, H. Seong, Y. N. Whang, and W. Hong, "Energy-efficient 5G phased arrays incorporating vertically polarized endfire planar folded slot antenna for mmWave mobile terminals," *IEEE Trans. Antennas Propag.*, vol. 68, no. 1, pp. 230–241, Jan. 2020.

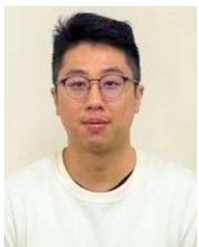

YIN CHEN CHANG received the B.S. degree from the Department of Electrical Engineering, National Taiwan Ocean University, Keelung City, Taiwan, in 2018. He is currently pursuing the master's degree with National Chiao Tung University, Taiwan, where he is working as Research Assistant, under the supervision of Prof. J.-H. Tarng. His main field of research includes millimeter-wave antennas, array antennas, and antenna in package. His current research interests include 5G mobile antennas, wideband antennas, and antenna array for millimeter-wave applications.

CHING CHENG HSU received the B.S. degree from the Department of Electrical Engineering, National Chung Cheng University, Taiwan, in 2016, and the M.S. degree from the Department of Communications Engineering, National Chiao Tung University, Taiwan, in 2018, where he is currently pursuing the Ph.D. degree in communication engineering. His research interests include MMW antenna design, ultrawideband antenna, and antenna in package.

M. IDREES MAGRAY (Graduate Student Member, IEEE) received the B.Tech. degree in electronics and communication engineering from the Islamic University of Science and Technology, Awantipora, in 2018. He is currently pursuing the master's degree with National Chiao Tung University, Taiwan, where is working as Research Assistant, under the supervision of Prof. J.-H. Tarng. He received INAE Fellowship for two months and during that tenure he worked under the supervision of Prof. S. K. Koul. He worked on various projects with CARE, IIT Delhi, under the guidance of Prof. S. K. Koul. He has authored or coauthored several articles in peer-reviewed journals and conference proceedings. His research interests include co-designed 4G/5G antennas for smartphones, mmWave antennas for mobile terminals and base stations, and antenna-in-packaging. He received the Best Project Competition Award in InCAP 2019.

HSU YUNG CHANG received the B.S. degree from the Department of Electrical Engineering, National Taiwan Ocean University, Keelung City, Taiwan, in 2018. He is currently pursuing the master's degree with National Chiao Tung University, Taiwan, where he is also working as a Research Assistant, under the supervision of Prof. J.-H. Tarng. His main research field is millimeter-wave 5G antennas, end-fire mobile antenna design, and antenna-in-package consideration for millimeter-wave applications.

JENN-HWAN TARNG (Senior Member, IEEE) is a Professor with the Department of Electrical Engineering and the Dean of the College of Electrical and Computer Engineering, National Chiao Tung University. He was on leave to the Industrial Technology Research Institute (the largest government funded research) as the General Director of ISTC from 2007 to 2011, and Service Systems Technology Center (merging two other centers) from 2011 to 2016. He is currently the Co-PI of the Center for mmWave Smart Radar Systems and Technologies (a flag-ship project), where he is also the PI of the sub-project entitled "Large and Scalable mmWave Digital Phased Antenna Array." He has published more than 100 referred journal papers and conference papers. His research interests include in antennas, RFIC design, radio channel modeling and measurement, and RFID/Internet of Things.